arXiv:1603.03147v1 [cond-mat.supr-con] 10 Mar 2016

Vortex shells in mesoscopic triangles of amorphous superconducting thin films

N. Kokubo[1], H. Miyahara[1], S. Okayasu[2], T. Nojima[3]

[1]*Department of Engineering Science, University of Electro-Communications, Cho-fugaoka 1-5-1, Cho-fu, Tokyo 182-8585, Japan*
[2]*Advanced Science Research Center, Japan Atomic Energy Agency, Tokai, Ibaraki 319-1195, Japan*
[3]*Institute for Materials Research, Tohoku University, Sendai 80-8577, Japan*

Abstract

Direct observation of vortex states confined in mesoscopic regular triangle dots of amorphous MoGe thin films was made with a scanning superconducting quantum interference device microscope. The observed magnetic images illustrate clearly how vortices are distributed over the triangle dots by forming not only commensurate triangular clusters, but also unique patterns imposed by incommensurability. We discuss the results in terms of vortex shells and construct the packing sequence of vortices in the multiple shell structure.

Keywords: Mesoscopic superconductors, Vortex Matter, Shell structures, Scanning SQUID microscope
PACS: 74.25.Qt, 74.25.Fy

1. Introduction

The confinement of a few vortices into small superconductors provides an opportunity to study fundamental properties of finite two-dimensional clusters in a lateral confinement. In a circular shaped, superconducting small dot, vortices near the edge are aligned in a ring(s) along its boundary, while those near the disk center form a triangular cluster. These structural ordering compete with each other and the resulted vortex arrangement is determined by the interplay between the geometry-induced confining potential and the mutual repulsive interaction between vortices [1, 2, 3, 4]. For large vorticities, a piece(s) of the triangular vortex lattice remains near the disk center because of densely packed vortices [3, 5], whereas for small vorticities, vortices are arranged themselves into regular polygons situated on concentric circular rings from the disk center [1, 2, 4]. This is called "vortex shells", of which configurations have been visualized by some experimental studies on mesoscopic superconducting disks of Nb and amorphuous MoGe thin films [6, 7].

The issue of vortex shells would be interesting when vortices are confined in polygonal small superconductors like triangle [8, 9, 10], square [11, 12] and pentagonal shaped dots [13]. These polygonal dots have discrete, natural symmetries that coincide or compete with the configurational symmetry of vortex polygons, depending on vorticity L. In triangle dots, vortices intrinsically form a triangular cluster of which symmetry is commensurate with that of the triangle geometry. This appears when voriticity is equal to one of triangle numbers, i.e. $L = n(n+1)/2$ with

an integer n. For other cases, the vortex state is frustrated with the geometry, and a metastable state(s) with free energy close to one for the ground state is created [8, 9].

Recently, we have reported the direct observation of multi-vortex states in triangle shaped, mesoscopic dots of weak pinning amorphous thin films with a scanning superconducting quantum interference device (SQUID) microscope [10]. We observed the coexistence of multiple (metastable) patterns at some vorticities. It turns out that the configurational degeneracy can be lifted by introducing some deformation in the triangle geometry, i.e., the transformation from regular triangles to isosceles ones. The observed vortex patterns were characterized by the two-fold reflection symmetry (incommensurate states) or the three-fold symmetry (commensurate states), and they were interpreted as either a commensurate triangular pattern, a linear vortex chain(s) or their combination for L up to 11.

In this study, we extend the previous work not only to study vortex states in equilateral triangle dots for L more than 11 (up to 15), but also to understand whether vortex arrangements can be interpreted in terms of vortex shells, as seen in circle and square dots [7, 12].

2. Experimental

We used a laboratory-built rf magnetron sputtering system to deposit amorphous Mo_xGe_{1-x} films ($x \approx 75\%$) with 0.20 μm thickness on Si substrates glued on a water cooled sample stage. By employing conventional UV lithography and chemical/dry etching techniques, we patterned the films into not only arrays of triangular dots for imaging, but also long bridges for transport measurements. The latter were used to obtain characteristic parameters of the films as follows: The superconducting transition temperature T_c is 6.0 K, a slope of the second critical field S in the vicinity of T_c is $\sim$ 2.3 T/K, and the normal resistivity at 10 K is $\sim$ 1.6 $\mu\Omega$m. Using the dirty-limit expression given in Ref. [15], the coherence length at zero temperature $\xi(0)$ and the penetration depth $\lambda(0)$ were estimated to be 5 nm and 0.5 μm, respectively.

We used a commercial scanning SQUID microscope (SQM-2000, SII Nanotechnology) with a magnetic sensor chip integrating the Nb-based dc-SQUIDs (Nb/Al-AlO_x/Nb Josephson junctions) and an inductively coupled, small Nb-pickup loop. A homogeneous magnetic field was applied perpendicularly to the sample surface using a coil wound in our sample stage. The sample stage has three stepper motors which allow us to approach and scan the samples in scales of μm with respect to the magnetic sensor. The vortex images presented in this study were taken on equilibrium vortex states prepared by the field-cool procedure, in which the magnetic field was applied in some temperatures ($\sim$ 15 K) above T_c, followed by cooling the samples in the magnetic field to temperatures of 3–4 K ($< T_c$) for imaging [7].

3. Results and Discussions

Figures 1(a)–1(o) show vortex images for vorticities L = 1–15 observed in 92 μm equilateral triangle dots. These images clearly illustrate individual vortices with reasonable spatial and magnetic resolutions. A piece of the triangular lattice is stably formed when the vorticity becomes the triangular number, i.e., L = 3 [Fig. 1(c)], 6 [Fig. 1(f)] 10 [Fig. 1(j)], and 15 [Fig. 1(o)]. As seen partly from traced patterns in Figs. 1(a')–1(o'), vortex arrangements are explainable in terms of the formation of triangular vortex shells. After forming a triangle configuration at L = 3, the vortex configuration evolves with vorticity as follows; $\cdots \rightarrow (1, 3) \rightarrow (5) \rightarrow (6) \rightarrow (1, 6) \rightarrow (1, 7) \rightarrow (1, 8) \rightarrow (1, 9) \rightarrow (2, 9) \rightarrow (2, 10) \rightarrow (2, 11) \rightarrow (3, 11) \rightarrow (3, 12)$. Here, we employ the

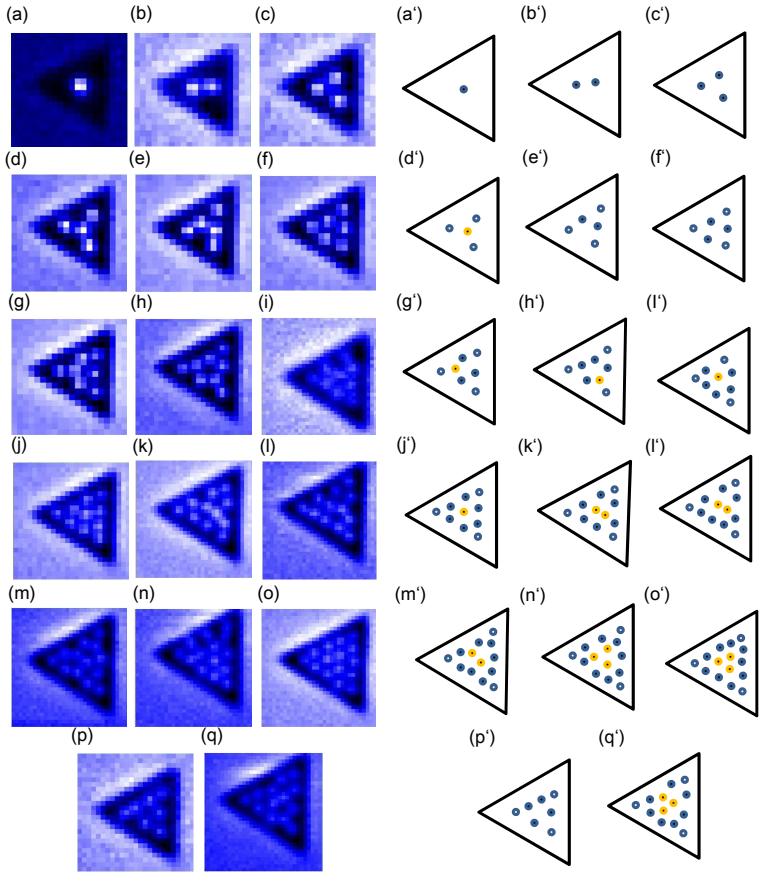

Figure 1: Scanning SQUID microscopy images of vortices in 92 μm equilateral triangular dots for vorticities L = 1–15 observed at different magnetic fields of (a) 0.50, (b) 1.50, (c) 2.50, (d) 3.00, (e) 3.50, (f) 4.00, (g) 4.50, (h) 4.80, (i) 5.40, (j) 5.75, (k) 6.15, (l) 6.20, (m) 6.78, (n) 6.80, (o) 7.50, (p) 4.40 and (q) 6.75 μT. The traced vortex patterns are given in (a')–(q').

standard notation for multiple shells characterized by $(N_1, N_2, \cdots, N_i)$ where N_i is the occupation of vortices in i-th shell from the center. Unlike quantum atoms where new electrons are added only in the most outer shell, both shells are filled with vortices by increasing L.

Many metastable states are created by the incommensurability between the geometry and vorticity: At $L = 7$, a single shell of (7) appears [Figs. 1(p) and 1(p')], in addition to a double shell configuration (1, 6) with a single vortex "core" [Figs. 1(h) and 1(h')]. At $L = 11$ (also $L = 12$), two configurations of double shells were observed; one has a single vortex core, as seen in the previous study [Figs. 2(l) and 2(x) in Ref. [10]], and the other has a vortex-pair core shown in Figs. 1(k) and 1(k'). At $L = 13$ (also $L = 14$), double shell configurations have either pair [Figs. 1(m) and 1(m')] or triangle cores [Figs. 1(q) and 1(q')], but the metastability disappears at the commensurate vorticity of $L = 15$. These vortex configurations are summarized in Table 1.

Table 1: Vortex configurations observed in mesoscopic dots with different shapes

L	Configuration		
	Triangle	Square [12]	Disk[7]
1	(1)	(1)	(1)
2	(2)	(2)	(2)
3	(3)	(3)	(3)
4	(1, 3)	(4)	(4)
5	(5)	(1, 4), (5)	(5)
6	(6)	(1, 5)	(1, 5)
7	(1, 6), (7)	(1, 6)	(1, 6)
8	(1, 7)	(1, 7)	(1, 7)
9	(1, 8)	(1, 8)	(1, 8)
10	(1, 9)	(2, 8)	(2, 8)
11	(2, 9),(1, 10)	(3, 8)	(3, 8)
12	(2, 10),(1, 11)	(4, 8)	(3, 9)
13	(2, 11),(3, 10)	(4, 9)	(3, 10)
14	(3, 11),(2, 12)	(4, 10)	(4, 10)
15	(3, 12)	(4, 11)	(5, 10)
16		(4, 12)	(5, 11[a])
17		(1, 4, 12)	(1, 5, 11[a])

[a] A vortex(vortices) trapped at the dot edge is ignored.

Focusing on the evolution of vortex configuration with vorticity, we find that a single shell structure is formed not only for $L = 1$–3, but also $L = 5$ and 6. It is worth recalling that a triangle pattern at $L = 6$ is commensurate with the triangle geometry and does not accompany any observable metastable state(s). Thus, the formation of the single shell structure after forming the double shell structure at $L = 4$ is robust, and therefore the packing sequence of vortices in multiple shells is not monotonic with vorticity.

This feature is also visible in Fig. 2(a), where the occupations of vortices in different shells are plotted against vorticity. After a monotonic increase of the occupation N_1 of the first shell up to 3 (at $L = 3$), it drops to 1 due to the formation of double shell structure at $L = 4$. With further increasing L, however, the single shell structure is reformed, and the corresponding occupation

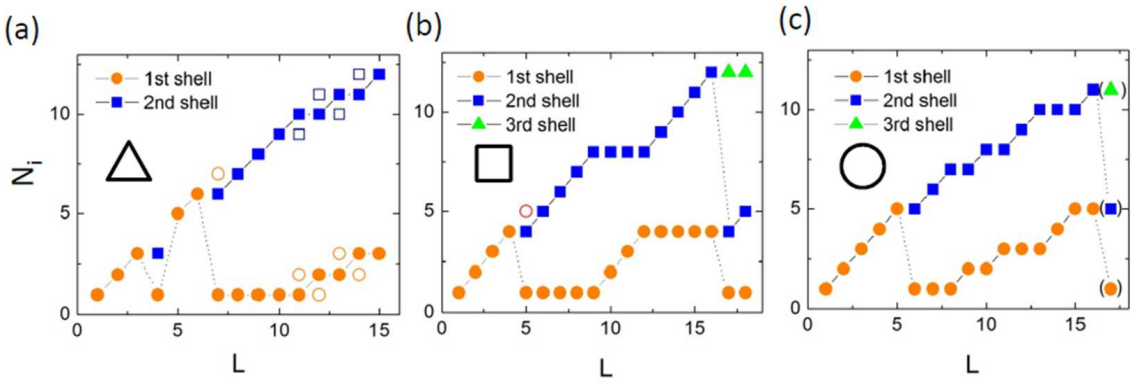

Figure 2: Figure 2 (Color online) Occupation N_i of different shells vs vorticity L for (a) triangle, (b) square [12], and (d) circle dots [7]. Open symbols denote vortex configurations observed less frequently. Lines are guide to eye.

N_1 jumps to 5 at $L = 5$ and takes the maximum value of 6 at $L = 6$. The second shell is also discontinuous with vorticity. After the first appearance of the second shell with $N_2 = 3$ at $L = 4$, it disappears at $L = 5$ and 6, above which N_2 reappears and increases monotonically with L.

It is worth noting that in mesoscopic square and circle dots the occupation of the first shell is "repeated" in their packing sequences. As seen from Fig. 2(b), in the square dots, the occupation N_1 in the first shell varies from 1 to 4 for $L = 1$–4, and this repeats for $L = 5$–16 [12]. In the circle dots [Fig. 2(c)], the variation of N_1 is also repeated in a range from 1 to 5 [4, 7]. These features indicate the presence of the maximum occupation of the first shell, and allow us to define closed shell configurations for both dot geometries. Namely, (4) and (4, 12) are closed configurations for square dots, while (5) and (5, 11) are for circle dots, as listed in Table 1. The situation is different in the triangle dots. As seen from Fig. 2(a), N_1 varies from 1 to 3 for $L = 1$–3, while it does from 5 to 6 for $L = 5$–6. This non-monotonic behavior of N_1 seems repeatable, when one takes into account vortex configurations for $L \geq 16$ observed in a numerical simulation [9]. As seen from Fig. 3 in Ref. [9], double shell configurations with V-shaped core ($N_1 = 5$) or triangle one ($N_1 = 6$) appear for $L = 19$–22, after the formation of a triple shell configuration ($N_1 = 1$) at $L = 18$. Thus, N_1 varies from 1 to 6 for $L = 7$–22, but $N_1 = 4$ remains missing.

The reason for the non-monotonic feature in mesoscopic triangle dots originates simply from the fact that four vortices do not form a square-like shell pattern due to the influence of the dot geometry. Otherwise, N_1 would vary monotonically from 1 to 6 and the closed shell configuration were uniquely defined as (6), which correspond to a stable, commensurate triangle state at $L = 6$. This may lead to an argument if a triangle pattern with one vortex in the center is regarded as (1, 3) or (4).

There is another filling rule of vortex shells, which is based on the assumption that three vortices situated near the corners of the triangle dot form the outermost shell [8]. This model characterizes the triangle pattern at $L = 6$ as a double shell configuration of (3, 3). The V-shaped pattern at $L = 5$ becomes a (2, 3) configuration. As a result, the corresponding packing sequence becomes monotonic with vorticity as follows: $\cdots \rightarrow (1, 3) \rightarrow (2, 3) \rightarrow (3, 3) \rightarrow (4, 3) \rightarrow (5, 3) \rightarrow (1, 5, 3) \rightarrow (1, 6, 3) \rightarrow (1, 7, 3) \rightarrow \cdots$. Thus, after the formation of (1, 3) at $L = 4$, double shell configurations continue up to $L = 8$, above which triple vortex shells appear. We note that the

inner parts of configurations (ignoring three vortices in the outermost shell) are similar to ones in disks, i.e., $\cdots \rightarrow (1) \rightarrow (2) \rightarrow (3) \rightarrow (4) \rightarrow (5) \rightarrow (1, 5) \rightarrow (1, 6) \rightarrow (1, 7) \rightarrow \cdots$. Thus, the observed vortex patterns (for $L > 3$) can be regarded as the combination of three corner vortices and "concentric" shell configurations, but the resultant occupations of multiple shells are not repeatable due to the limited occupation of the outermost shell.

4. Summary

We have presented SQUID images of vortex states confined in mesoscopic regular triangle dots of weak pinning amorphous MoGe films for vorticities L = 1–15. The formation of a triangular vortex cluster occurs at the triangle numbers of vorticities (L = 3, 6, 10 and 15), while for other vorticities, vortex patterns are mostly frustrated with the dot geometry, and form unique arrangements, including metastable ones, determined by the incommensurability between the geometry and vorticity. Irrespective of the (in)commensurability, the observed vortex arrangements are explainable in terms of vortex shells. The corresponding packing sequence reveals that the single shell structure is stably reformed after the formation of the double shell structure. Thus, closed shell configurations are not uniquely defined, in contrast to the results in mesoscopic circle and square dots [7, 12]. We believe that the observed feature is not related to the metastability, but intrinsic to mesoscopic triangle dots.

Acknowledgment This work was supported by JSPS KAKENHI Grant Numbers 23540416, 26287075 and 26600011, Nanotechnology Network Project of the Ministry of Education, Culture, Sports, Science and Technology (MEXT), and the Inter-university Cooperative Research Program of the Institute for Materials Research, Tohoku University (Proposal No. 14K0004).

References

[1] A. I. Buzdin, J. P. Brison: Phys. Lett. A **196** (1994) 267-271.
[2] B. J. Baelus and F. M. Peeters, Phys. Rev. B **65**(2002) 104515 (12 pages).
[3] L. R. E. Cabral, B. J. Baelus, and F. M. Peeters, Phys. Rev. B **70**, 144523 (2004).
[4] V. R. Misko , B. Xu, F M. Peeters, Phys. Rev. B **76** (2007) 024516 (11 pages).
[5] N. R. Cejas Bolecek, M. I. Dolz, A. Kolton, H. Pastoriza, C. J. van der Beek, M. Konczykowski, M. Menghini, G. Nieva, Y. Fasano, J. Low Temp. Phys. 179 (2015) 35 (7 pages)
[6] I. V. Grigorieva, W. Escoffier, J. Richardson, L. Y. Vinnikov, S. Dubonos, V. Oboznov, Phys. Rev. Lett. **96**, 077005 (2006).
[7] N. Kokubo, S. Okayasu, A. Kanda, B. Shinozaki,Phys. Rev. B **82** (2010) 014501(8 pages).
[8] H. J. Zhao, V. R. Misko, F. M. Peeters, V. S. Oboznov, V. Dubonos, I. V. Grigorieva, Euro Phys. Lett. 83 (2008) 17008 (6 pages).
[9] L. R. E. Cabral, B. J. Baelus, F. M. Peeters, Phys. Rev. B **70** (2009) 144523 (13 pages).
[10] N. Kokubo, H. Miyahara, S. Okayasu, T. Nojima, J. Phys. Soc. Jpn. **84** (2015) 043704 (4 pages).
[11] H. J. Zhao, V. R. Misko, F. M. Peeters, V. S. Oboznov, V. Dubonos, I. V. Grigorieva,Phys. Rev. B 78 (2008) 104517 (11 pages)
[12] N. Kokubo, S. Okayasu, T. Nojima, H. Tamochi, B. Shinozaki, J. Phys. Soc. Jpn., **83** (2014) 083704(5pages).
[13] H. T. Huy, M. Kato, T. Ishida, Supercond. Sci. Technol. **26**(2013) 065001 (11 pages).
[14] E. Zeldov, A. I. Larkin, V. B. Geshkenbein, M. Konczykowski, D. Majer, B. Khaykovich, V. M. Vinokur, and H. Shtrikman, Phys. Rev. Lett. **73** (1994) 1428-1431.
[15] P. H. Kes and C. C. Tsuei, Phys. Rev. B 28 (1983) 5126-5139.